Mon. Not. R. Astron. Soc. **301,** 179–192 (1998)

A spectral decomposition of the variable optical, ultraviolet and X-ray continuum of NGC 5548

Paweł Magdziarz,[1⋆] Omer M. Blaes,[2] Andrzej A. Zdziarski,[3] W. Neil Johnson[4] and David A. Smith[5]

[1]*Astronomical Observatory, Jagiellonian University, Orla 171, Cracow, Poland*
[2]*Department of Physics, University of California, Santa Barbara, CA 93106, USA*
[3]*N. Copernicus Astronomical Center, Bartycka 18, 00-716 Warsaw, Poland*
[4]*Naval Research Laboratory, Code 7651, 4555 Overlook Ave. SW, Washington, DC 20375-5352, USA*
[5]*NASA/GSFC, Code 668, Greenbelt, MD 20771, USA*

Accepted 1998 July 24. Received 1998 May 22; in original form 1997 December 20

ABSTRACT

We present an analysis and decomposition of the broad-band optical/UV/X-ray/γ-ray spectrum of the Seyfert 1 galaxy NGC 5548. The spectrum consists of an average of simultaneous optical/*IUE*/*Ginga* observations accompanied by *ROSAT* and *CGRO*/OSSE data from non-simultaneous observations. We show that the overall optical/UV/X-ray/γ-ray spectrum can be deconvolved into three basic continuum components: a cool multitemperature blackbody, a hard thermal Comptonized component and an EUV/soft X-ray component well described by a thermal Comptonization continuum. Assuming that the optical/*IUE* spectrum comes from a cold disc, the maximum disc temperature is very well constrained by the data to be $kT_{\rm disc} = 3.2^{+0.2}_{-0.2}$ eV. This rules out models explaining the soft excess as a far tail of the disc spectrum. We show that the soft excess inferred by the data requires a separate continuum component, which is consistent with thermal Comptonization in optically thick ($\tau \sim 30$), warm ($\sim$0.3 keV) plasma. This Comptonization component contains a significant fraction of the source energy. The plasma parameters of the hard continuum ($\tau \sim 2$, $kT_{\rm HC} \sim 50$ keV) are consistent with those suggested for the average spectrum of Seyferts.

On the basis of the broad-band spectral model, we also re-analyse the simultaneous *IUE*/*Ginga* campaign. We find that the fluxes in all three continuum components are positively correlated. The total flux emitted in the hard component is positively correlated with both the spectral index and the solid angle of cold matter seen by the hot source. Such a correlation suggests that the variability mechanism is related to changes in the geometry of the continuum-emitting regions, and an excess in the amount of reflection requires deviations from a simple plane disc picture. The variations in the hard spectral index can then be explained by increased cooling of the hot plasma caused by the increased number of seed photons. We suggest that the geometry variations may be related to a transition region between a cold and a hot disc.

Key words: accretion, accretion discs – galaxies: individual: NGC 5548 – galaxies: Seyfert – ultraviolet: galaxies – X-rays: galaxies.

1 INTRODUCTION

The optical/UV/X-ray continuum spectrum of NGC 5548 is typical of type 1 Seyferts, and consists of three main components: the big blue bump, the soft X-ray excess (modified by a warm absorber) and the hard X-ray power law with reflection hump and high-energy cut-off. These components are known to be highly variable, but there have been no observing campaigns that cover all three simultaneously. The relationship between them is therefore currently uncertain.

The big blue bump is commonly believed to be thermal emission from a multitemperature accretion disc, but this explanation has problems. The long-wavelength portion of the bump is softer (redder) than $F_\nu \propto \nu^{1/3}$, the expected behaviour for a stationary accretion disc. In addition, Hopkins Ultraviolet Telescope data show no absorption or emission edge at the Lyman limit (Kriss et al. 1997). Both of these problems plague accretion disc models of Seyfert galaxies and quasars in general (e.g. Barvainis 1993; Blaes 1998; Krolik 1998).

The hard X-ray spectrum is explained rather well by thermal Comptonization of the UV accretion disc continuum by a hot

⋆Deceased 1998 August.

corona. Much of the accretion power might be dissipated in this corona (Haardt & Maraschi 1991), and part of the big blue bump could then arise from reprocessing of the X-rays by the disc. Strong support for this picture comes from the existence of the Compton reflection feature and the fact that the iron Kα line is broad (Mushotzky et al. 1995; Nandra et al. 1997). This also explains the fact that the optical and UV emission vary together in a correlated fashion with the hard X-rays, within time-scales of the order of several days (Clavel et al. 1992). Occasionally, however, there are uncorrelated UV outbursts which may be caused by variations in the accretion rate of the disc (Clavel et al. 1992). A possible problem with disc–corona models is that they may give rise to large Lyman emission edges. This is because of the high density in the accretion disc atmosphere that results when power is taken out of the disc and placed in the corona (Sincell & Krolik 1997).

The soft X-ray excess in NGC 5548 and in Seyfert 1 galaxies in general is perhaps the least understood component of all. The few existing variability studies that include this component have produced confusing and possibly conflicting results. Done et al. (1995) studied variability of the soft X-ray excess and the hard power law, but only in the narrow 0.1–2 keV *ROSAT* band. During their monitoring campaign, which spanned two months, the soft X-rays underwent a flare on a time-scale of $\sim$8 d. There was no corresponding increase in the hard X-ray power law. This suggests that the two components are decoupled on short time-scales some of the time. In contrast, Marshall et al. (1997) presented *EUVE* light curves which overlapped with *IUE*, *HST* and ground-based optical data (Korista et al. 1995). They found that the EUV flux, which is associated with the soft X-ray excess, varied simultaneously with the optical/UV fluxes, and with larger amplitude. Their observations spanned 8 d and they did not detect any time lag between the EUV and UV fluxes down to the observational limit of 0.25 d. Given that the optical/UV photons are known usually to exhibit correlated variability with the hard X-rays, as noted above, one would expect that the soft excess would correlate with the hard X-ray flux. Such a correlation was, in fact, detected previously in *EXOSAT* monitoring data by Kaastra & Barr (1989) on a $\sim$1-d time-scale of observations. They also found a delay of $\sim$5000 s in the hard X-ray variability with respect to the soft X-rays. However, interpretation of the *EXOSAT* data is still unclear, owing to instrumental problems. The reality of the soft/hard X-ray delay, as well as signatures of quasi-periodicity found by Papadakis & Lawrence (1993), has been found to be questionable (Tagliaferri et al. 1996). It may be that there is both correlated and uncorrelated variability, the latter perhaps being caused by enhanced dissipation in the accretion disc. Such dissipation has been suggested as an explanation of the residual UV flux (with respect to that resulting from reprocessing) in NGC 4151 (Zdziarski & Magdziarz 1996; Warwick et al. 1996). The residual flux in NGC 4151 shows probable variability on time-scales of the order of months.

The soft excess has often been interpreted as the high-energy extension of the big blue bump (e.g. Walter & Fink 1993). In addition to the problems they face in the optical/UV, simple thin accretion discs that radiate as multitemperature blackbodies cannot explain the soft excess, although it may be that more complicated atmosphere models could work (e.g. Czerny & Elvis 1987). Haardt, Maraschi & Ghisellini (1994) have suggested that flaring regions in a patchy corona on the disc might store accretion energy for a time before discharging it, thereby producing local bright spots on the disc. These spots might give rise to a soft excess. Variability in such a model has been explored by Haardt, Maraschi & Ghisellini (1997), but, as they point out, it is not clear whether the model can be made fully consistent with the lowest hardness ratio reported in the *ROSAT* band for NGC 5548 by Done et al. (1995). An important clue to the nature of the soft excess is that it appears to have a universal spectral shape in Seyferts (Walter & Fink 1993; Walter et al. 1994). This could be explained as being the result of atomic physics, e.g. if the soft excess were produced by reflection in an X-ray photoionized skin of the accretion disc (Ross & Fabian 1993; Matt, Fabian & Ross 1993; Czerny & Życki 1994; Życki et al. 1994). However, this model provides a poor fit to the spectra of high-luminosity sources (Fiore, Matt & Nicastro 1997). In addition, there is no evidence in the *EUVE* data for the strong emission lines expected from photoionization processes (Marshall et al. 1997).

Several groups have attempted in the past to construct models of NGC 5548 that explain all the continuum components together, with varying degrees of success. Kaastra & Barr (1989) concluded from their analysis of *EXOSAT* monitoring observations that the soft excess is produced by the inner parts of the disc and the variability and soft/hard X-ray time lag are caused by radial propagation of thermal instabilities towards the centre. Walter & Courvoisier (1990) also examined *EXOSAT* variability data, including ground-based optical and *IUE* observations. Most of these data were non-simultaneous, but they were useful for examining long-term trends. Walter & Courvoisier concluded that an accretion disc plus a stratified conical wind with a shock provided a good description of the data. Loska & Czerny (1997) examined simultaneous optical, *IUE* and *Ginga* data, and concluded that an accretion disc with an inner radius cut-off and corona, or a distribution of optically thin clouds, explained the data equally well.

In this paper we re-analyse the available archival data in order to construct, for the first time, a detailed broad-band continuum model of the emission from the nucleus of NGC 5548, and attempt to constrain the geometry and physical emission mechanisms of the continuum components. We improve over previous work by performing a full spectral decomposition, permitting us to examine in detail the relation between the shapes and energetics of the different components. Our data consist of spectra from a simultaneous optical/*IUE*/*Ginga* campaign (Clavel et al. 1992; Nandra et al. 1993), supplemented by *ROSAT* (Done et al. 1995) and OSSE (Johnson et al. 1997a) non-simultaneous observations. Using a recently improved reduction of the *Ginga* data, we also re-analyse the variability of the spectral components in the *Ginga* campaign. In addition, we discuss *EXOSAT* monitoring observations (Branduardi-Raymont 1986, 1989; Turner & Pounds 1989; Kaastra & Barr 1989; Nandra et al. 1991) in the context of our broad-band spectral model. Section 2 discusses the data reduction and analysis, Section 3 presents the average broad-band spectrum and deconvolved continuum, and Section 4 presents correlations in the flux variability obtained on the basis of the broad-band model. In Section 5 we discuss physical models of the central engine suggested by our analysis, and compare our results with previous work. In all the analysis in this paper we adopt a redshift of 0.0166 for NGC 5548 (e.g. Walter & Courvoisier 1990). Using a Hubble constant of $\simeq$75 km s^{-1} Mpc^{-1} the distance is $d \simeq 70$ Mpc.

2 OBSERVATIONAL DATA

2.1 Simultaneous optical/UV/X-ray data

After searching the available public data bases, we have found optical, ultraviolet, and hard X-ray data that are nearly simultaneous for nine epochs, listed in Tables 1–3. The optical data are

Table 1. Optical data from Peterson et al. (1992) simultaneous with the *Ginga* 1989–1990 observing campaign.

Epoch	Julian Date (−244 0000)	F_λ (5100 Å) (10^{-15} erg s^{-1} cm^{-2} Å^{-1})
1 (Jan 89)	7535	10.16 ± 0.41
	7539	10.74 ± 0.38
2 (Jan 89)	7556	9.08 ± 0.32
3 (Jun 89)	7685	9.52 ± 0.38
4 (May 90)	8036	7.73 ± 0.43
	8037	8.06 ± 0.26
5 (May 90)	8039	7.78 ± 0.43
	8040	8.18 ± 0.45
	8041	8.08 ± 0.44
6 (Jun 90)	8047	7.84 ± 0.47
7 (Jun 90)	8056	7.95 ± 0.32
8 (Jun 90)	8068	6.96 ± 0.23
9 (Jul 90)	8077	6.53 ± 0.26

Table 2. *IUE* data simultaneous with the *Ginga* campaign.

Epoch	Data file	Julian Date at start (−244 0000)	Exposure time (s)
1	SWP35323	7538.17012	5100
	SWP35324	7538.26546	4800
	SWP35325	7538.35485	4800
	LWP14802	7538.23831	3599
2	SWP35461	7557.15933	3600
	SWP35462	7557.24372	3600
	LWP14945	7557.20728	2700
3	SWP36411	7684.92897	4500
	SWP36412	7685.01944	1500
	LWP15670	7684.88740	3000
	LWP15671	7684.98760	2099
4	SWP38870	8037.37957	4800
	LWP17990	8037.33148	3600
5	SWP38881	8039.32074	4500
	SWP38882	8039.42044	2700
	SWP38903	8040.83304	4800
	LWP18006	8039.37745	3300
	LWP18009	8040.89591	3600
6	SWP39019	8048.40843	5400
	LWP18035	8048.47959	3900
7	SWP39082	8055.42914	4199
	SWP39083	8055.52896	2400
	LWP18093	8055.48368	3300
8	SWP39153	8068.73464	5100
	SWP39154	8068.84789	1800
	LWP18197	8068.80128	3600
9	SWP39175	8076.67044	6000
	LWP18284	8076.74743	3180

from the ground-based observations reported by Peterson et al. (1992), and show the flux measured at a rest wavelength of 5100 Å. The ultraviolet data files come from the *IUE* electronic archives (reprocessed with NEWSIPS). The *Ginga* data come from the monitoring campaign reported by Nandra et al. (1991). The largest non-simultaneity between the different wavelength regions occurs during epoch 1, where the ultraviolet and X-ray data are separated by nearly 2 d. In addition, the only optical data available for this particular epoch come from a day earlier and a day later than the observing time of the ultraviolet and X-ray observations.

Table 3. *Ginga* data simultaneous with the available *IUE* data.

Epoch	Julian Date at start (−244 0000)	Julian Date at end (−244 0000)	Exposure time (s)	Count rate at 2–10 keV (count s^{-1})
1	7536.34037	7537.41741	5120	11.9±0.1
2	7555.22926	7557.12556	28928	20.7±0.1
3	7685.18486	7686.33449	12672	18.7±0.1
4	8035.87852	8037.50074	21248	15.8±0.1
5	8038.81532	8041.41681	10112	15.2±0.1
6	8047.77704	8048.87628	14464	12.7±0.1
7	8054.37611	8055.75093	17792	20.7±0.1
8	8068.42677	8069.45936	12416	9.8±0.1
9	8075.03949	8076.41727	18304	8.0±0.1

2.1.1 *Ginga data*

We extracted data from both the top layer and the mid layer of the LAC (Large Area Counter) detector (cf. Smith & Done 1996 for a description of the background subtraction and reduction procedure). The mid layer gives a larger effective area above ∼10 keV, which is crucial for determining the Compton reflection component. That layer had previously been ignored because of problems with background subtraction. However, a recently improved reduction procedure gives reliable results. We ignore the first three channels of the top layer, which restricts the low-energy data to > 1.7 keV, and the first 20 channels of the mid layer, which are affected by background subtraction and give no significant area below 10 keV compared with the top layer. The observation log is given in Table 3.

In order to understand new information carried by the mid-layer data, we first re-analysed the total 12-epoch *Ginga* data set from Nandra et al. (1991) and compared it against previous results. We apply a model consisting of a power law with high-energy cut-off, Compton reflection (Magdziarz & Zdziarski 1995), a Gaussian line and an ionized absorber implemented as an ABSORI model in XSPEC version 9 (Arnaud 1996), and based on that of Done et al. (1992). The ionization parameter is defined by $\xi = Ln^{-1}r^{-2}$ erg s^{-1} cm^{-1}, where L is the 5-eV to 20-keV luminosity in the incident spectrum and n is the density of the absorber located at distance r from the illuminating source. Throughout this paper, we use abundances from Anders & Ebihara (1982), and express the ionization coefficient in units of erg cm s^{-1}. The absorber temperature is fixed at 10^5 K (Krolik & Kallman 1984). We assume that the inclination of the disc is $i = 30°$, the expected average for Seyfert 1s (e.g. Nandra et al. 1997). This makes the Compton reflection component harder in the 10–20 keV range compared with the average reflection model by Lightman & White (1988) applied in Nandra et al.'s (1991) original analysis. We fix, a posteriori, the high-energy cut-off at $E_{\rm HC} = 100$ keV (cf. Section 2.2.2), and include absorption from a fixed neutral column density along the line of sight of 1.65×10^{20} cm^{-2} per hydrogen atom (Nandra et al. 1993). The mid-layer detector has a larger effective area over 10 keV than the top-layer detector, and this gives a more reliable determination of the spectral index and the contribution from Compton reflection. We obtain an average flux spectral index ($F_\nu \propto \nu^{-\alpha}$) of $\alpha_{\rm HC} = 0.78^{+0.04}_{-0.03}$ at $\chi^2/\nu = 42/44$ d.o.f. (Errors are calculated throughout this paper at a 90 per cent confidence limit for one parameter, which corresponds to $\Delta\chi^2 = 2.7$.) This is significantly harder than $\alpha = 0.91 \pm 0.07$ found by Done et al. (1995) for the same data set. Nandra et al. (1991) applied an iron line which was self-consistent with the Compton reflection component, and obtained $\alpha = 0.85 \pm 0.05$. Our data averaged over 12 observing epochs give a well-determined

Compton reflection component fitted independently of the iron line: the solid angle covered by the reflector as seen from the X/γ source, divided by 2π sr, is $R = 0.74^{+0.14}_{-0.17}$. Such a fit requires a substantially ionized warm absorber: $\xi = 1500^{-500}_{+700}$ erg s^{-1} cm^{-1} with $N_{\rm H} = (3.5^{+1.1}_{-1.2}) \times 10^{22}$ cm^{-2}.

The fit still shows a clear residuum in the low-energy range of the spectrum around 2 keV. This cannot be compensated for by high ionization of the absorber, and presumably comes from the soft excess component, previously inferred to exist in *EXOSAT* data (Kaastra & Barr 1989) and *ROSAT* data (Walter & Fink 1993; Done et al. 1995). Such a soft component has also been detected in *ASCA* data (George et al. 1998). Including an additional power law with cut-off and fixed spectral index $\alpha_{\rm SE} = 1.2$ (Walter et al. 1994), we obtain a significantly better fit with χ^2 erg s^{-1} cm^{-1}= 29/42 for a softer spectral index $\alpha_{\rm HC} = 0.86 \pm 0.06$ and amount of reflection $R = 0.96^{+0.23}_{-0.18}$. The fitted cut-off energy of the soft excess component is $E_{\rm SE} = 0.59^{+0.05}_{-0.14}$ keV, and no other constraints on the shape can be made from the *Ginga* data, which only extend down to 2 keV. The data show no significant ionization of the reflecting medium: $\xi_{\rm R} = 0^{+0.2}$ erg s^{-1} cm^{-1}. This is consistent with the previous analysis by Done et al. (1995), and rules out models with substantial ionization of the disc surface. However, decomposition of the iron line and the Compton reflection depends significantly on the modelling of the continuum (Zdziarski, Johnson & Magdziarz 1996), and is substantially affected by relativistic effects superposed on the reflection component (Matt, Perola & Piro 1991; Maciołek-Niedźwiecki & Magdziarz 1998). The ionized absorber inferred by the data allows at most a moderate ionization coefficient of $\xi = 0^{+24}$ erg s^{-1} cm^{-1} with fitted column density $N_{\rm H} = (2.1^{+0.9}_{-1.0}) \times 10^{22}$ cm^{-2} when we include the soft excess component. However, a zero-ionization absorber with a standard gas-to-dust ratio would be inconsistent with an assumption of a common UV/X-ray absorber, because the UV flux would then be blocked, unless there is substantial clumpiness, i.e. partial covering. The parameters of the ionized absorber we fitted are inconsistent with those derived by Mathur, Elvis & Wilkes (1995) for a unified UV/X-ray warm absorber and those suggested by George et al. (1998) from *ASCA* 1993 data (Mushotzky et al. 1995). This may be related to the fact that in both papers the soft excess was not taken into account. In fact, George et al. (1998) obtained a better fit, which is more consistent with ours, by approximating the soft excess as a soft power law. However, their parameters still show the ionized absorber to be weaker than our preliminary fit to the *Ginga* data without the soft excess component. This suggests some variability of the ionized absorber on a time-scale of years (cf. Done et al. 1995), or that the models of the warm absorber are still far from physical (see Kallman 1998 for a discussion of the observability of detailed features in the warm absorber).

Our fit still has some residuum in the region of the iron edge. However, this cannot be removed by our model, and the data give no constraints on the iron abundance. For further analysis, we separate a 9-epoch subset from Nandra et al.'s (1991) data set (Table 3), which is accompanied by simultaneous optical and *IUE* observations. Our model fits the total co-added 9-epoch data with the continuum described by $\alpha_{\rm HC} = 0.79^{+0.06}_{-0.07}$, $R = 0.68^{+0.23}_{-0.21}$, $E_{\rm SE} = 0.60^{+0.05}_{-0.11}$ keV, and the warm absorber with $\xi = 0^{+46}$ erg s^{-1} cm^{-1}, and $N_{\rm H} = (2.2^{+1.0}_{-1.2}) \times 10^{22}$ cm^{-2} at $\chi^2/\nu = 42/42$.

2.1.2 *Optical and IUE data*

Optical/UV spectra for each of our nine epochs were produced in the following way. We replaced all bad pixels in the *IUE* spectra with linear interpolation between neighbouring good pixels. For those epochs in Tables 1 and 2 that have multiple observations, we took an error-weighted average to combine the data together. We then assigned errors equal to the greatest standard deviation of the individual measurements at each wavelength, or the greatest difference between the individual measurements, whichever was larger.

Since we are interested in both the spectral shape of the optical/UV continuum and the total luminosity of this component compared with the X-rays, it is very important to correct the data properly for interstellar extinction. Unfortunately, the amount of extinction is uncertain, and there is even disagreement in the literature on the foreground Galactic contribution. In view of this, we consider two extreme possibilities. The first is that the reddening is entirely negligible and the second is that there is an intrinsic $E(B-V) = 0.05$ in the nucleus of NGC 5548 itself (cf. discussion in Walter & Courvoisier 1990). We neglect Galactic reddening in both cases.

The *IUE* wavelengths were transformed to the rest frame of NGC 5548, and then starlight subtraction was performed in the following way. We adopted a 5100-Å (in the rest frame of NGC 5548) starlight flux of $(3.4 \pm 0.4) \times 10^{-15}$ erg s^{-1} cm^{-2} Å^{-1} in the standard optical aperture of 38 arcsec^2 (Romanishin et al. 1995), and scaled an M31 bulge template spectrum (Coleman, Wu & Weedman 1980) to give the same flux at this wavelength. We then subtracted the starlight spectrum from the optical/UV data, taking into account the difference in apertures between the *IUE* cameras and the ground-based observations. These aperture corrections were based on the V-band aperture photometry of the underlying galaxy in table 1 of Romanishin et al. (1995). The SWP and LWP apertures admit 2.30 ± 0.09 and 2.27 ± 0.1 times more V-band starlight flux, respectively. The starlight contribution was less than 2 per cent in the SWP data and 11 per cent in the LWP data. The SWP and LWP data for each epoch were then joined together by eliminating the noisier LWP data in the wavelength region of overlap. Finally, the data were combined with the corresponding optical fluxes. For the case where we consider reddening by the nucleus of NGC 5548, the data were then dereddened using the extinction curve of Cardelli, Clayton & Mathis (1979), assuming $R_V = 0.31$. Note that we did not include any reddening corrections in the starlight subtraction phase of the analysis, implying that any reddening is located well within the nucleus itself. Given that the starlight corrections are small in the *IUE* data, and that they are based on a direct measurement at 5100 Å, we believe our results will be insensitive to this issue.

We wish to concentrate on the continuum spectrum of NGC 5548 in this paper, and we therefore have to remove the contributions of the broad-line region from the optical/UV spectra. We did this by first taking an unweighted average of the spectra from all nine epochs, adopting as errors at a particular wavelength just the average of the individual errors. We then fitted this spectrum to a simple accretion disc continuum plus multiple Gaussians for the following emission lines: geocoronal Lyα, Lyα, N v λ1240 (including its absorption feature, cf. Clavel et al. 1991), O i λ1304, Si iv+O iv] λ1402, C iv λ1549, He ii λ1640, O iii] λ1663, C iii] λ1909 and Mg ii λ2798. We also included a number of broad Gaussians to fit the Fe ii pseudocontinuum around the Mg ii λ2798 line. We adopted a Shakura & Sunyaev (1973) accretion disc model for the continuum, assuming each annulus of the disc radiates locally as a blackbody. The specific flux is given by

$$F_\nu = \frac{4\pi R_{\rm g}^2 h\nu^3 \cos i}{d^2 c^2} \int_6^\infty {\rm d}r \frac{r}{\exp(h\nu/kT) - 1}, \qquad (1)$$

where the local surface temperature T is given by

$$T^4 = \frac{3GM\dot{M}}{8\pi R_g^3 \sigma r^3}\left[1 - \left(\frac{6}{r}\right)^{1/2}\right], \quad (2)$$

r is the radius in units of the gravitational radius $R_g \equiv GM/c^2$, M is the mass of the black hole, $\dot{M}$ is the accretion rate, and all other symbols have their usual meanings. Only two parameters are required to specify the accretion disc continuum, $M^2 \cos i$ and $\dot{M}/M^2$. Equations (1) and (2) are admittedly very crude representations of the spectrum likely to emerge from a realistic accretion disc, and neglect substantial radiative transfer and relativistic effects. We intend to fit the data to more realistic models (cf. Agol, Hubeny & Blaes 1998) in a future paper.

Fig. 1 depicts the average optical/UV spectrum and fit for the case with no dereddening. The fit to the line fluxes is not perfect, particularly at the longest wavelengths of the LWP data, where there remains some Fe II flux. The continuum fit gives $M \simeq 9 \times 10^7 (\cos i)^{-1/2}$ $M_\odot$ and $\dot{m} \simeq 0.04(\cos i)^{-1/2}$ (where $\dot{m} \equiv \dot{M}c^2/L_{Edd}$), implying a maximum disc temperature of 2.9 eV. For the case with dereddening corresponding to $E(B-V) = 0.05$, we find instead $M \simeq 8 \times 10^7 (\cos i)^{-1/2}$ $M_\odot$ and $\dot{m} \simeq 0.06(\cos i)^{-1/2}$, giving a maximum disc temperature of 3.3 eV. In both cases, these parameters are similar to those of the accretion disc fits to the ultraviolet data of Krolik et al. (1991), although they assumed an extreme Kerr hole and obtained somewhat higher maximum disc temperatures. Even so, as noted by those authors, the temperatures are far too low to explain any soft X-ray excess with a simple bare disc model. As we stated in the Introduction, the ultraviolet spectrum of NGC 5548 is redder than $F_\nu \propto \nu^{1/3}$, the long-wavelength prediction for a bare disc. It is therefore only possible to fit the spectrum with a simple bare disc model if the disc temperature is very low. The resulting spectral curvature allows one to explain the fact that the spectrum hardens as the source gets brighter (Molendi, Maraschi & Stella 1992; Loska & Czerny 1997).

We used the line and continuum parameters of these fits to the average spectra as initial trial values to fit the spectra and subtract the line fluxes for each individual epoch. Next, we converted all of the optical and UV continuum data into XSPEC pha format using a unitary diagonal response matrix. We refitted the average (over all epochs) dereddened data with the disc spectrum using the maximum disc temperature as a parameter of the fit. The model overestimates the flux at the optical 5100-Å point, which suggests that the reddening is slightly overestimated. Next, we implemented Cardelli et al.'s (1989) extinction curve in an XSPEC model and refitted the optical/UV data assuming free extinction. The fit constrains very well the maximum disc temperature $kT_{disc} = 3.16^{+0.17}_{-0.15}$ eV and extinction $E(B-V) = 0.029^{+0.016}_{-0.015}$, showing that the continuum is well determined from the data despite some residuals coming from inaccurate line subtraction.

Note that the temperature derived here is a temperature that

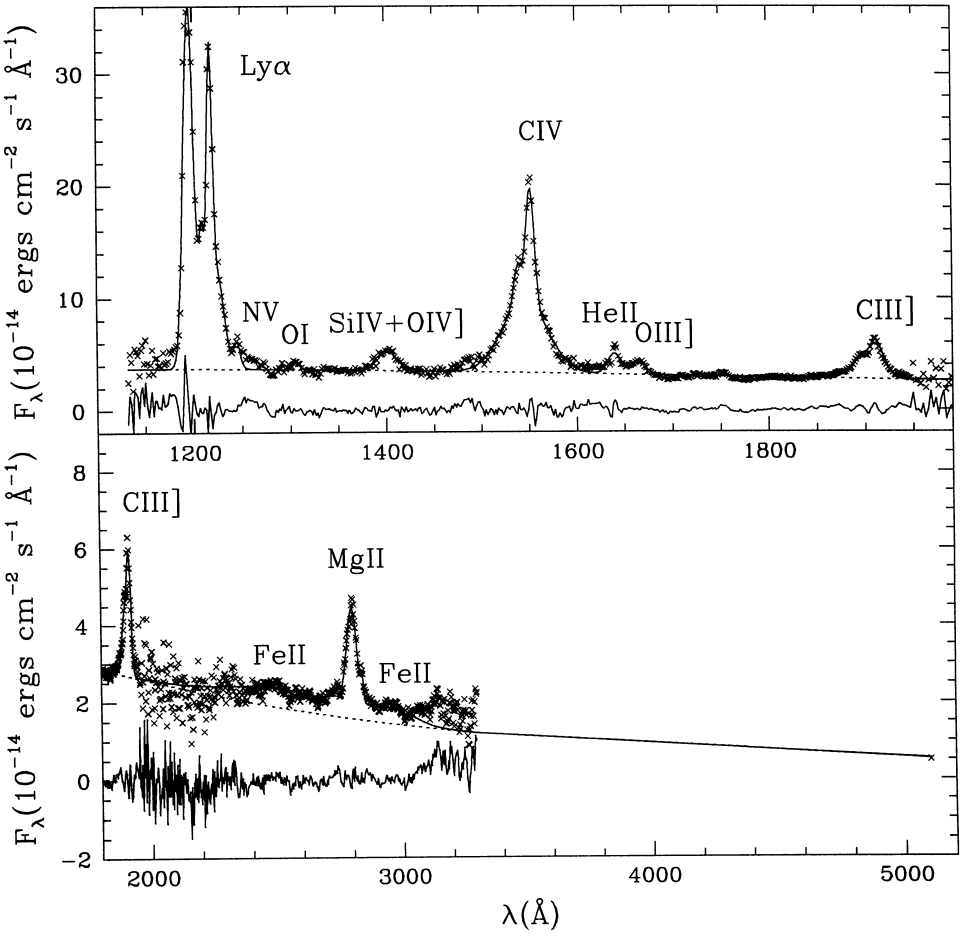

Figure 1. Average optical/UV spectrum (crosses) from all nine epochs (cf. Tables 1 and 2). Error bars have been suppressed for clarity. The solid curve through the data points represents our best-fitting continuum and emission-line model. The dashed line shows the continuum alone. The residuals to the fit are plotted in the lower solid curve. No correction for reddening has been applied to the data or the fit in this figure.

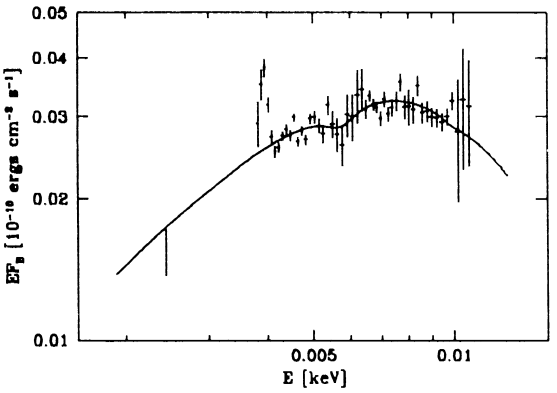

Figure 2. The average optical/UV continuum from all nine observing epochs with no correction for reddening. The *IUE* spectrum has been rebinned by a factor of 20. The solid line shows our model, consisting of a reddened multiblackbody disc spectrum. The inflection between 5 and 6 eV is caused by the 2200-Å bump in the reddening curve. Enhanced residua below 4 eV come from inaccuracy in the subtraction of the Fe II pseudocontinuum and those near 10 eV are caused by poor subtraction of the Lyα line (cf. Fig. 1).

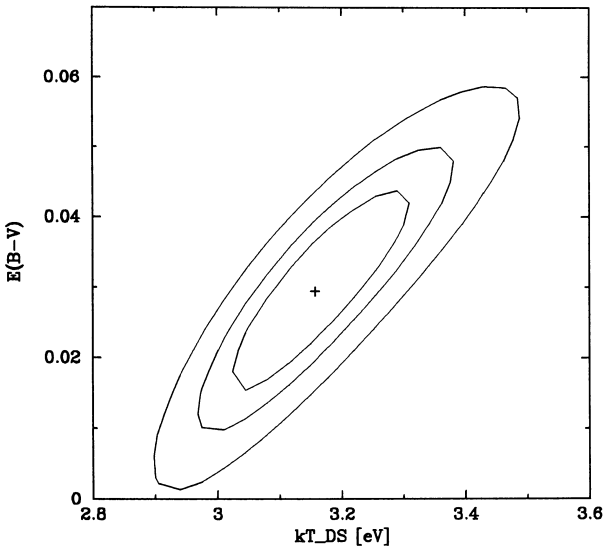

Figure 3. Confidence contours at 68, 90 and 99 per cent (for two parameters) for the maximum disc temperature and $E(B-V)$ in the average optical/UV continuum.

describes the average disc spectrum. It is therefore not a physically well-defined average maximum temperature of the disc itself. However, both quantities are closely related to each other, a fact which we tested a posteriori. This confirms our derivation of $E(B-V)$, which has a value consistent with that resulting from the average relation between hydrogen column density and reddening, assuming the same neutral absorber as observed in X-rays. This result is related to the fact that the system parameters may be asymptotically treated as linear, given the limited variability dynamics with respect to the statistical uncertainties, which makes the analysis of average spectra reasonable. Generally, this conclusion is not always true. The problem appears mostly in X-ray data, since they are affected by poor photon statistics, and thus they require photon accumulation over long time intervals. However, taking into account confidence limits of fitted parameters, such a description is usually successful (e.g. Zdziarski et al. 1995; Gondek et al. 1996). Here, we treat averaging of the UV and X-ray broad-band data consistently in the same way, and the spectral parameters calculated should be understood as parameters of the average spectrum rather than average parameters.

Fig. 2 shows the spectrum after rebinning the original *IUE* data by a factor of 20, and the fitted model. The long- and short-wavelength residua in the *IUE* data range come from inaccuracies in the Fe II pseudocontinuum and Lyα subtraction, respectively. These do not affect the fit, however. The optical point is still marginally overestimated, which cannot be corrected by our model. This may indicate some inaccuracies in the relative calibration of the instruments, but more exotic continuum models cannot be rejected. Fig. 3 shows confidence contour plots in the $E(B-V)-kT_{\rm disc}$ plane. The data clearly reject disc models with maximum temperatures higher than a few eV, and thus do not allow for production of the soft excess from a disc component. This conclusion has been reached previously by Kuraszkiewicz, Loska & Czerny (1997). They deconvolved a large sample of optical/UV observations of NGC 5548, and, on the basis of an accretion disc/corona model by Witt, Czerny & Życki (1997), derived parameters of the disc entirely consistent with ours.

Additional inaccuracy in the determination of the internal optical/UV emission may come from the so-called FC2 continuum, which may contribute to the observed continuum in a manner which is difficult to deconvolve. The presence of such additional continuum coming from extended regions has been reported in a number of active galactic nuclei (AGNs) (cf. Antonucci 1993; Paltani & Walter 1996). Kuraszkiewicz et al. (1997) found that the FC2 continuum in NGC 5548 at $H\beta$ does not account for more than 20 per cent at the faintest states of the source and drops down to a few per cent in bright states. Taking into account that a linear decomposition of the *IUE* spectrum (Paltani & Walter 1996; on the basis of principal component analysis: Kendall & Stuart 1976) gives a constant component which is softer than the variable continuum, one would expect that the contribution from FC2 will not significantly affect the UV continuum at its maximum, which, therefore, effectively limits the maximum disc temperature during the fit. At the faintest historically observed *IUE* state of NGC 5548, the contribution to the *IUE* spectrum from a linearly deconvolved constant component was about 50 per cent at the low-energy range of the LWP camera, dropping down to a few per cent at the high-energy range of the SWP camera (Done, private communication). This, in fact, gives an upper limit to the contribution from an extended continuum source, since the accretion disc is not a linear system and the maximum temperature changes in a correlated fashion with the total emitted flux (cf. Fig. 8b later).

2.2 Non-simultaneous data

2.2.1 ROSAT 1992 December–1993 January campaign

Until now, the best analysis of the soft X-ray energy range for NGC 5548 has been that presented by Done et al. (1995) on the basis of the *ROSAT* 1992 December–1993 January campaign. However, this campaign was not associated with any observations by hard X-ray instruments, and this means that results on spectral variability are very uncertain, given the low-energy resolution response matrix of the *ROSAT* PSPC detector. Done et al. (1995) found the best fit to the average campaign data with a double blackbody model of the soft excess. We refitted the average *ROSAT* spectrum with both the double blackbody model and the cut-off power-law model which we applied to the *Ginga* data set (cf. Section 2.1.1). All the *ROSAT* PSPC data that we analyse in this paper have had a 2 per cent error

added to account for instrumental systematics (cf. Done et al. 1995; see also Osborne 1993 for a discussion of the *ROSAT* systematic errors). The double blackbody model constrains the spectral index of the hard component well, giving a value $\alpha_{\rm HC} = 0.83^{+0.08}_{-0.10}$ at $\chi^2/\nu = 8.8/21$. The model needs an ionization coefficient for the absorber of $\xi = 3700^{+\infty}_{-3000}\,{\rm erg\,s^{-1}\,cm^{-1}}$ and a column density $N_H = (9^{+14}_{-8}) \times 10^{22}$ cm^{-2}. Such parameters are within the confidence limits of the fit to the *Ginga* data when assuming no soft excess component. This is, however, not consistent with the contribution of the soft excess to the the lowest energy channel of the *Ginga* data. Taking into account the contribution from the soft excess in the *Ginga* range, the data instead suggest variability in the ionized absorber on a time-scale of years.

On the other hand, we find that the cut-off power-law model fits the *ROSAT* data equally well with $\chi^2/\nu = 9.5/23$, despite its rather artificial form. Replacing the cut-off power-law with a more physical thermal Comptonization spectrum (Lightman & Zdziarski 1987), we obtain a better fit with $\chi^2/\nu = 8.5/23$. We find that the Comptonization model does not constrain the hard continuum spectral index, and so we fix it at the value of $\alpha_{\rm HC} = 0.86$ derived from the fit to the total *Ginga* data set (cf. Section 2.1.1). The spectral index of the soft excess is well constrained by the *ROSAT* average data to be $\alpha_{\rm SE} = 1.13^{+0.18}_{-0.10}$, which is consistent with the index found by Walter et al. (1994) from an analysis of simultaneous *IUE* and *ROSAT* data obtained during the All Sky Survey. The same value of $\alpha_{\rm SE}$=1.1 holds for the average spectrum from the simultaneous 1993 March–May observing campaign with *IUE* and *EUVE* (Korista et al. 1995; Marshall et al. 1997). The data weakly constrain the temperature of the soft excess, giving $kT_{\rm SE} = 0.56^{+0.40}_{-0.32}$ keV, which results mostly from a degree of freedom in the fit related to the relative normalization between the soft and the hard continuum. The relatively low resolution of the PSPC cannot constrain such a normalization in the spectral shape. Limited energy resolution also makes the fit to the *ROSAT* data dependent on unresolved details of the ionized absorber and possible line emission. The Comptonization model fitted to the *ROSAT* data gives an ionization coefficient $\xi = 45^{+13}_{-30}\,{\rm erg\,s^{-1}\,cm^{-1}}$, which is well within the confidence limits of the *Ginga* results, but with a marginally consistent column density $N_{\rm H} = (0.8^{+0.2}_{-0.2}) \times 10^{22}$ cm^{-2}, in contrast to the double blackbody model. This result is again inconsistent with the fits to the *ASCA* data (George et al. 1998; cf. Section 2.1.1). We conclude that *ROSAT* distinguishes poorly between the various spectral shapes of the continuum. The fact that Done et al. (1995) were able to determine the hard component reasonably well came from applying specifically the double blackbody model. In the case of the Comptonization model, we can determine the spectral index of the soft excess, but no constraints can be made on the hard continuum.

The soft excess spectral index observed in the *ROSAT* data is generally much steeper than that observed in the hard continuum component. On the other hand, Fiore et al. (1994) found a systematic difference of $\sim$0.5 between PSPC and Einstein IPC spectral indices for a sample of radio-quiet quasars. If this is true, the fitted soft X-ray spectral index may be systematically too soft, and correcting for this may reduce the spectral index to a value consistent with that of the hard continuum. This may substantially change the physical parameters of the soft excess inferred by the data. However, it cannot remove the soft excess completely, since a clear residuum is detected in the *Ginga* data and the presence of the soft excess was established independently by *EXOSAT* data (Kaastra & Barr 1989; Nandra et al. 1991). In addition, George et al. (1998) found a significant improvement in fitting *ASCA* 1993 data when they included a soft X-ray power law of $\alpha \sim 3.2$. While such a power law provides a good description of the soft excess in the limited *ASCA* bandpass, it is inadequate once the *ROSAT* data are considered. The *ROSAT* data show clear curvature in the soft X-rays (Done et al. 1995), which rules out an extrapolation of a soft power law below $\sim$0.5 keV. The curvature in the soft X-ray spectrum is also suggested by *EUVE* variability (Marshall et al. 1997). George et al. (1998) claim that the *ASCA* data show essentially a power-law shape with subtle upturns at both the very lowest and very highest energies. Such a spectrum cannot be deconvolved properly given contributions to the underlying hard continuum from a soft excess of unknown nature and from a Compton reflection component, and it is no surprise that their double power-law model is able to mimic such a spectral shape adequately. This fit cannot be directly compared with our continuum model, given the complex picture of the warm absorber seen with *ASCA*, and we intend to discuss the soft X-ray continuum in a forthcoming paper (Magdziarz et al., in preparation).

As discussed in the Introduction, Done et al. (1995) found significant variability in the *ROSAT* monitoring data, which showed different behaviour in the soft and hard spectral ranges. By comparing the count rate ratio for various epochs, they showed that the soft excess component is highly variable during moderate changes in the hard power law, which is in contradiction to reprocessing models. However, the *ROSAT* data poorly determine the spectral shape, and thus such variability does not necessarily mean that the soft and hard continuum are decoupled, especially given the lack of hard X-ray data in their analysis (e.g. spectral changes in the hard component could compensate for the total flux observed in the 1–2 keV *ROSAT* range). We fit the monitoring data for each epoch separately with the Comptonization model determined from the average spectrum. However, the quality of the data does not allow for determination of spectral shape variations. The soft X-ray spectral index is consistent with being constant within large statistical uncertainties, and no constraints can be made on the temperature and the hard power law for the individual epochs.

2.2.2 *OSSE data*

In order to determine the energetics of the hard continuum, we also analyse archival *GRO*/OSSE observations. The OSSE data constrain the high-energy rollover of Seyfert spectra well, and so we can determine the cut-off energy assuming the continuum to be produced by thermal Comptonization (e.g. Zdziarski et al. 1997). We consider here the OSSE spectra from observing Phase 1 and Phase 3. Phase 1 consists of viewing periods 7.5 (1991 August 17–23), 12 (1991 October 19–31) and 13 (1991 November 2–7). Phase 3 consists of viewing periods 302 (1993 September 8–10) and 303.2 (1993 September 23–October 2). All up-to-date data and their analysis are presented in Johnson et al. (1997a). The data are probably affected by a systematic error of unknown nature at 560 keV, so we ignore everything above the 40th OSSE channel.

We fit the spectra from Phases 1 and 3 with a cut-off power law, which is a good approximation to the thermal Comptonization high-energy tail observed in Seyferts by the OSSE detectors (Johnson et al. 1997a; Zdziarski et al. 1997). Our analysis gives no constraints on the spectral index, but freezing the spectral index and reflection to $\alpha_{\rm HC} = 0.86$ and $R = 0.96$ respectively (the results obtained from analysis of the *Ginga* data; cf. Section 2.1.1) gives a cut-off energy of $E_{\rm HC} = 120^{+630}_{-70}$ keV at $\chi^2/\nu = 36/38$ for Phase 1 and $E_{\rm HC} = 118^{+160}_{-50}$ keV at $\chi^2/\nu = 28/38$ for Phase 3. The poor constraint on the high-energy limit for Phase 1 comes from poor

statistics. Both data sets show the same cut-off energy within the statistical uncertainties, and they provide a good determination of the high-energy rollover of the spectrum, thereby giving limits on the energetics of the source. The total apparent flux in the hard continuum component is $F_{\rm HC} = 0.38^{+0.42}_{-0.13}$ keV cm^{-2} s^{-1} for Phase 1 and $F_{\rm HC} = 0.61^{+0.36}_{-0.18}$ keV cm^{-2} s^{-1} for Phase 3, assuming a frozen $\alpha_{\rm HC}$ and R. The flux difference between Phases 1 and 3 comes entirely from the difference in the normalization, and there is no statistical reason to consider the spectra as different.

As our OSSE data give no constraints on the spectral shape, but are good enough to determine the rollover of the spectrum, we use a sum of the spectra from Phases 1 and 3 in all further analysis. Fitting simultaneously the total 12-epoch *Ginga* data (cf. Section 2.1.1) and the total OSSE data with free relative normalization, we obtain $E_{\rm HC} = 160^{+270}_{-70}$ keV at $\chi^2/\nu = 59/80$, which corresponds to $F_{\rm HC} = 1.79^{+0.33}_{-0.44}$ keV cm^{-2} s^{-1} at the normalization of the *Ginga* data set. Including the *Ginga* data makes the confidence limits for the cut-off energy wider, but it constrains the total flux emitted in the hard continuum component very well. On the basis of the above, we assume from now on that the high-energy cut-off of the hard continuum is relatively constant over the epochs of observation, and the γ-ray spectrum varies only in normalization. Similar behaviour is observed in NGC 4151 (Zdziarski et al. 1996; Johnson et al. 1997b) and other Seyferts (Zdziarski et al. 1997).

3 BROAD-BAND AVERAGE SPECTRUM

We first construct a baseline spectrum by averaging the simultaneous optical/*IUE*/*Ginga* data sets from all epochs together. The resulting spectrum gives the correct normalization between the optical/UV and X-ray spectrum, but it is insufficient for investigating the energetics of the source. The three components characteristic of the X-ray continuum of a Seyfert 1, namely the Comptonization continuum, Compton reflection and soft excess, are clearly observed in the spectrum. However, they cannot be deconvolved from the *Ginga* data alone (Nandra et al. 1991), even after we include results from the mid-layer detector (see below). In order to determine the relative contribution of each component of the average spectrum, we supplemented the *Ginga* observations with *ROSAT* and OSSE average data and fitted them simultaneously, assuming free normalization with respect to the optical/*IUE*/ *Ginga* average spectrum. The free normalizations account for both physical variability of the source and relative cross-calibration between the X-ray instruments. We neglect here the problem of unknown, a priori, cross-calibration uncertainties between the ultraviolet and X-ray instruments.

3.1 Broad-band X-ray/γ-ray spectrum

We found in Section 2.2 that OSSE data show variations in spectral normalization, but no dramatic variability in spectral shape. The energetics of the hard continuum in our composite spectrum are therefore well determined. We note that, generally, a cut-off energy depends on the spectral index (e.g. Zdziarski et al. 1996), and so fits with a frozen high-energy cut-off are usually unsuccessful. The fitted normalization of the OSSE spectrum is $C_{\rm OSSE} = 0.6^{+0.2}_{-0.1}$ with respect to the *Ginga* data, suggesting that the source was observed in a relatively faint state during the *Ginga* campaign. The *ROSAT* data fix the shape of the soft excess, the tail of which contributes to the *Ginga* spectrum. This contribution is weakly dependent on the soft excess shape, but allows the hard continuum spectral index to be established by the *Ginga* data. On the other hand, the *ROSAT* data poorly constrain the cut-off energy of the soft excess, which is, however, well determined from *Ginga*. The shape of the soft excess is also reasonably fixed by the *ROSAT* average spectrum, as the monitoring data show no significant variability of the spectral shape in the soft X-ray range (cf. Section 2.2.1 and Done et al. 1995). We expect that our composite X-ray/γ-ray spectrum is a reasonable approximation to the average spectrum, assuming that the source was not in dramatically different spectral states during the epochs when the non-simultaneous observations were collected.

We replaced the hard power-law continuum with a thermal Comptonization model (Lightman & Zdziarski 1987), because a power law is an insufficient approximation to the Comptonization continuum in both the high- and low-energy tails of the spectrum. We use a low-energy spectral index as the fitting parameter, rather than the geometry-dependent optical depth (cf. Zdziarski et al. 1996). The fit gives: $\alpha_{\rm HC} = 0.76^{+0.02}_{-0.03}$, $R = 0.31^{+0.21}_{-0.16}$, $kT_{\rm SE} = 280^{+70}_{-50}$ eV with $\chi^2 = 86/105$. We allowed the ionized absorber to be different in the *ROSAT* and *Ginga* data sets, because the data are non-simultaneous and show variations in both column density and ionization coefficient (cf. Section 2.2.1). The χ^2 obtained agrees within the limit of $\Delta\chi^2 = 2.7$ with the sum of the χ^2s resulting from fitting each data set separately, thus confirming that the data are statistically consistent with each other in the sense of our model. Most of the disagreement between the data is channelled into the amount of reflection, which appears to be underestimated in the broad-band fit. Such a fit is preferred because of the rescaling of the *ROSAT* data with a fitted factor $C_{ROSAT} = 0.7^{+0.07}_{-0.04}$, which shows that the source was brighter during the epoch of the *ROSAT* campaign than during the *Ginga* observations. As the X-ray spectrum is, generally, softer in bright states of the source (see Section 4 below), its rescaling down leads to a deficit of counts on the high-energy end of the *ROSAT* spectrum near 2 keV. This in effect makes the hard continuum detected by *Ginga* harder which is, finally, compensated for in the fit by underestimation of the reflection component. Such a situation may also be related to the soft X-ray flare reported by Done et al. (1995), which would make the tail of the *ROSAT* spectrum even softer. However, this does not change our qualitative conclusions, given that the total fit is statistically self-consistent.

The fit adequately deconvolves the hard continuum from the soft excess. However, the results should be treated carefully since averaging a highly variable spectrum is not equivalent to averaging strongly non-linear model parameters. We also checked, a posteriori, that in our composite spectrum the shape of the soft excess is still best described by an exponential energy cut-off or by a Comptonization tail when the hard continuum is fixed by the *Ginga* data. The fitted spectral index of the hard continuum lies in the tail of the Seyfert 1 distribution (Nandra & Pounds 1994), and, together with the temperature of the hot plasma and amount of reflection, is consistent with the continuum observed in the hard state of NGC 4151 (Yaqoob et al. 1993; Zdziarski et al. 1996), rather than the typical Seyfert 1.

3.2 Optical/UV/soft X-ray continuum

Next we included the optical/UV data and the accretion disc spectrum in the model. The disc temperature predicted from the optical/UV data is much too low to account for the soft X-ray range. We therefore tried a simple phenomenological model in which the soft excess arises from Comptonization of the disc spectrum. The fit gives $\alpha_{\rm SE} = 1.13^{+0.14}_{-0.12}$ and, as expected, does not alter the temperature of the soft excess obtained in the previous fit. The fit is

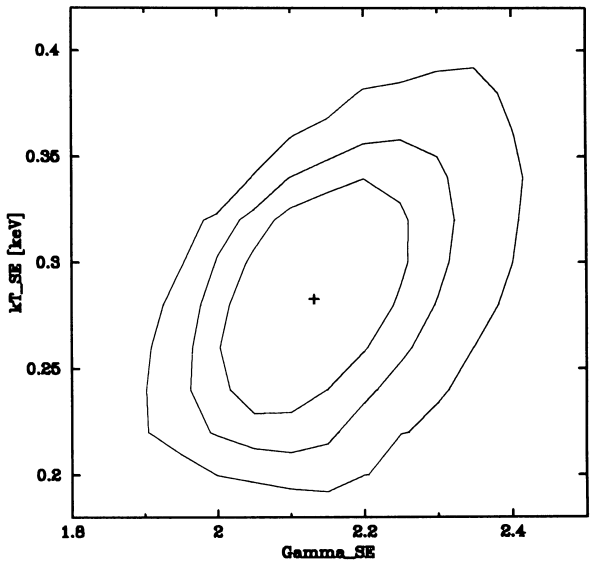

Figure 4. Contour plot of χ^2 on the plane of the soft excess plasma temperature $kT_{\rm SE}$ and photon spectral index $\Gamma_{\rm SE}(=\alpha_{\rm SE}+1)$ for the average *ROSAT*/*Ginga*/OSSE spectrum and the model including Comptonization of the soft excess photons to the hard continuum.

consistent with the previous results from simultaneous *IUE*/*ROSAT* observations reported by Walter et al. (1994). The optical/UV data alone allow, but do not require, the low-energy tail from the soft excess Comptonization component, because Comptonization does not significantly change the seed photon continuum (i.e. the disc spectrum). The presence of the Comptonized low-energy photons only moves the maximum temperature to a slightly lower value, $kT_{\rm disc}=2.5\pm0.3$ eV, than we obtained from fitting the optical/UV data alone (cf. Section 2.1.2). This effect is caused by the contribution to the UV spectrum from the soft X-ray Comptonization continuum, which is flatter than the blackbody tail above 0.01 keV (see Section 3.3 below), and thus leaves less room for the disc component in the total model. In the sense of our model, the disc temperature fitted in Section 2.1.2, assuming no contribution from the Comptonization tail, represents the maximum disc temperature allowed by the optical/UV data. From the point of view of the source structure, the presence of the low-energy tail from the soft excess Comptonization reduces the contribution of the cold disc to the total spectrum of seed photons seen by the hot Comptonizing source. Our model, in fact, decouples the relative normalization between the spectra of the blue bump and the soft X-ray components, allowing the relative normalization to be a free fit parameter, in contrast to models of high-temperature discs. This treatment also makes the fit relatively independent of the soft excess spectral index, constrained by the *ROSAT* data. This need not be, a priori, consistent with the optical/*IUE*/*Ginga* simultaneous data set, owing to both physical variability and the possible calibration uncertainties discussed in Section 2.2.1. On the other hand, the simultaneous optical/ *IUE*/*Ginga* data cannot constrain the relative normalization, because of the limited coverage of the soft excess component, and they leave an undetermined free parameter (see Section 4 below).

Depending on the source geometry, we might expect some photons from the soft excess to act as seed photons for Comptonization to the hard continuum (e.g. Kaastra & Barr 1989). Thus we include the soft excess in the Comptonization model, assuming as a free parameter a relative normalization between the seed photons from the disc and the seed photons from the low-temperature Comptonization describing the soft excess. Our data, however, cannot constrain such an effect, as the fit shows no significant changes in the spectral parameters with respect to the previous one, giving finally $kT_{\rm SE}=270^{+70}_{-50}$ eV, $\alpha_{\rm SE}=1.13^{+0.14}_{-0.11}$ for the soft excess, and $kT_{\rm HC}=55^{+210}_{-20}$ keV, $\alpha_{\rm HC}=0.76^{+0.01}_{-0.03}$, and $R=0.32^{+0.20}_{-0.17}$ for the hard continuum with $\chi^2/\nu=754/1113$. To make our determination of the soft excess parameters objective, we investigate the contours in the $kT_{\rm SE}$–$\alpha_{\rm SE}$ plane, ignoring the optical/UV data. Fig. 4 shows that the *ROSAT* average data determine the parameters of the Comptonization model quite reasonably in the presence of the hard continuum and the soft excess cut-off established by the *Ginga* spectrum. Thus predictions of our soft excess model are, a priori, consistent with the optical/UV data. Interestingly, the spectral index predicted for the soft excess leads to a significant contribution, or even domination, by the Comptonization component in the optical/UV range. This naturally explains the results of Marshall et al. (1997), who find a tight flux variability correlation between the *IUE* and *EUVE* data. The soft excess spectral index is also consistent with that resulting from the *IUE*/*EUVE* average spectrum.

3.3 Continuum and physical parameters

The resulting spectrum and its deconvolution into continuum components is presented in Fig. 5. The hard continuum gives Comptonizing plasma parameters of $kT_{\rm HC}\sim50$ keV and $\tau\sim2$, consistent with those typical of Seyfert 1s (Zdziarski et al. 1997). The parameters are determined using a Monte Carlo method (Pozdnyakov, Sobol' & Sunyaev 1983; Górecki & Wilczewski 1984) and assuming a uniform spherical source. Such a treatment allows us to translate geometry-independent parameters in the thermal Comptonization model of Lightman & Zdziarski (1987) into physical parameters of the plasma (cf. Zdziarski et al. 1996). It is energetically possible for the entire blue bump (the dot–long-dashed curve in Fig. 5b) to arise from reprocessing of the hard continuum, assuming the X/γ source forms a patchy corona above the surface of the disc. However, both the tight correlation in simultaneous *IUE*–*EUVE* data (Marshall et al. 1997) and the correlation of the soft X-rays with the hard continuum (Kaastra & Barr 1989) demand a physical connection between the soft excess and the disc/corona system. In addition, the low-energy extrapolation of the *ROSAT* soft X-ray power law crosses the UV continuum level (cf. Walter & Fink 1993), which is consistent with our assumption of the Comptonization origin of the soft excess. The blue bump then turns out to be dominated by Comptonization (the short-dashed and the dot–short-dashed curves in Fig. 5b), and contains about half of the total flux, which may still be consistent with the assumption of reprocessing after adjusting the source geometry. If this is the case, a proper deconvolution of the optical/UV/soft X-ray component appears to be the most crucial problem for determining the energetics of the source.

Since the fitted temperature of the soft excess plasma is non-relativistic and not much higher than that of the seed photons, the Comptonization process is nearly unsaturated, despite the extreme optical depth required by the spectrum ($\tau\sim30$). Such an optical depth is consistent, however, with that typical for an accretion disc, and suggests that the soft excess may come from Compton scattering within the disc itself (Czerny & Elvis 1987; Ross, Fabian & Mineshige 1992; Done et al. 1995). On the other hand, such a high optical depth may lead to an important contribution from bremsstrahlung which we cannot resolve from the observational

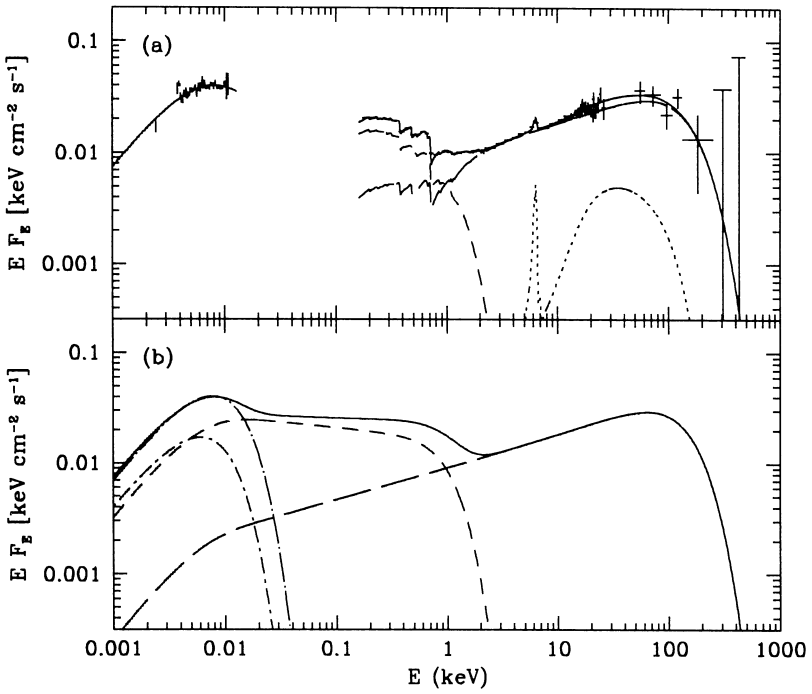

Figure 5. The intrinsic (i.e. after the effect of Galactic absorption at the soft excess and reddening at the optical/UV spectrum have been removed) broad-band average optical/UV/X/γ spectrum of NGC 5548. Panel (a) shows the data and fitted model, and panel (b) shows the decomposition of the spectrum into the disc and thermal Comptonization continuum components. Both *ROSAT* and OSSE data were fitted with free normalizations with respect to the simultaneous optical/*IUE*/ *Ginga* data set, and renormalized on the figure. The energy scale of the plot is in the source frame. The dot–short-dashed and short-dashed curves show the disc and the soft excess components, respectively. The soft excess component comes from optically thick Comptonization and dominates the spectrum from the optical/UV up to 1 keV. The long-dashed and dotted curves show the thermal Comptonization X/γ continuum and the reflection component, respectively. The dot–long-dashed curve shows the disc component fitted to the optical/*IUE* data separately.

data. A pure bremsstrahlung spectrum, however, is rejected by our data at high significance. Moreover, our approximation using single-temperature Comptonization may not be appropriate, as the plasma may be stratified in temperature and optical depth (cf. Nandra et al. 1995). Such stratification of the plasma parameters may simply mimic our thick Comptonization fit even in the case where a significant part of the emission is optically thin. The resulting diversity in cold plasma parameters may also explain the lack of atomic signatures observed in the soft excess spectra (Fiore et al. 1994, 1997). The above conclusions lead to a picture of the soft excess produced by a complex continuum component, the nature of which cannot be determined from the data available now, and new multiwavelength campaigns are extremely important in order to solve this problem.

4 CORRELATIONS BETWEEN SPECTRAL COMPONENTS

Our broad-band model continuum finally consists of the cold (several eV) disc spectrum; the soft, low-temperature (several hundred eV) Comptonization continuum and the hard Comptonization continuum ($\sim$100 keV). We assume that the soft excess photons contribute to the seed photons for Comptonization in the hot plasma, although we cannot be certain that this is true from the available data. On the basis of the above model, we analyse the simultaneous subset of *IUE–Ginga* observations assuming a constant hot plasma temperature, which is suggested by the OSSE observations. The *Ginga* data only allow for a crude approximation of the soft excess component, since they are only marginally affected by its far tail. On the other hand, the model allows the UV continuum to be generally decoupled from the X-rays, thus leaving a model-dependent factor which determines the normalization of the soft excess. This factor cannot be determined from the *IUE*/*Ginga* data set without assuming some detailed model of the UV/soft X-ray continuum.

The hard X-ray continuum shows significant correlation between the total flux changes and the spectral index and amount of reflection (Fig. 6). A similar steepening of the hard continuum as the source brightens was also detected in the *EXOSAT* data (Nandra et al. 1991). We find in addition that the source geometry changes in such a way as to produce more reflection when the source is brighter and softer. The data give no significant information on the iron line variability (cf. Nandra et al. 1991).

The soft excess required by the *Ginga* data seems to vary in a correlated fashion with the total flux emitted by the X/γ continuum (Fig. 7a). This suggests that the soft excess component is related to reprocessing, in agreement with the tight UV/EUV correlation found by Marshall et al. (1997) and the soft X-ray/hard X-ray correlation found by Kaastra & Barr (1989). However, the cut-off energy of the soft excess inferred by the *Ginga* data is consistent with being constant over the hard continuum changes (Fig. 7b), which requires some temperature locking process. Such a process would partly explain why Seyfert galaxies (including NGC 5548) appear to have a universal soft excess spectral shape (Walter & Fink 1993; Walter et al. 1994). On the other hand, extrapolation of the soft X-ray flux of our *Ginga* data to the simultaneous *IUE* flux suggests that in some bright epochs the soft excess spectral index is

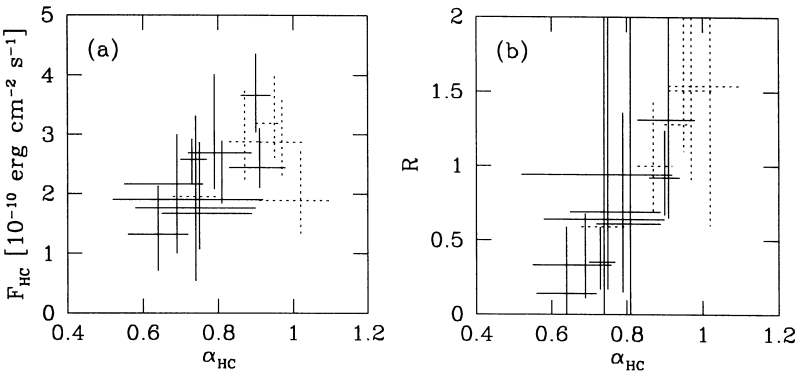

Figure 6. Correlation between the energy spectral index of the hard X/γ continuum and (a) its total flux emitted and (b) amount of reflection, i.e. the solid angle of cold matter seen by the X/γ source. When the source is brighter, it shows a softer spectral index and larger solid angle of cold matter intercepting the hard continuum. A Spearman rank-order correlation test gives confidence levels of 0.86 and 0.99 for α_{HC} versus F_{HC} and α_{HC} versus R, respectively. The dotted crosses mark results from the *Ginga* data that have not been accompanied by *IUE* observations.

rather harder than the canonical value of $\alpha_{SE} \approx 1.2$ fitted by Walter & Fink (1993), despite the fact that the average spectrum gives an index consistent with this result. The possibility of variability of the soft excess spectral index cannot be rejected. We note that the variability of the soft excess flux, combined with the fact that the hard X-rays are softer when brighter, might explain why Done et al. (1995) detected flaring in the soft *ROSAT* bandpass with little variation in the hard bandpass. This may also explain why George et al. (1998) detected an insignificant soft excess component in the *ASCA* data at > 0.6 keV, since the source was then rather bright ($F_{2-10} = 46 \times 10^{-12}$ erg cm^{-2} s^{-1}, compared with $F_{2-10} = 37 \times 10^{-12}$ erg cm^{-2} s^{-1} from our average *Ginga* data) and soft, which makes the hard tail of the soft excess more difficult to distinguish from the hard continuum.

The total flux emitted in the disc component is correlated with the hard X-rays (Fig. 8a; Nandra et al. 1993), again as expected under the assumption of reprocessing. The correlation appears at a confidence level of 0.96, which probably reflects both the systematic inaccuracies in the reduction and the various variability modes likely present in the UV and X-ray data (cf. results from the analysis of the observing campaign for NGC 4151, see Edelson et al. 1996). The correlation is consistent with being linear, and shows some residual flux in the hard X-ray component at zero UV flux. The residual flux is also visible in the correlation with the soft X-rays (Fig. 7a). This flux, however, turns out to be artificial when taking into account the fact that the total flux intercepted (and reprocessed) by the cold matter is dependent on the amount of reflection in the spectrum. The amount of reprocessed energy is roughly $\sim(1 - A)RF_{HC}$, with some additional factor depending on geometry ($2 \cos i$ for a simple disc geometry). The albedo A is roughly ~ 0.3, depending on the spectral shape of the hard continuum. The amount of reflection R is positively correlated with the spectral index (Fig. 6b) and with the total flux emitted in the hard continuum. However, the second correlation is less pronounced, because our data do not constrain the high-energy range of the spectrum, which dominates the energetics. The correlation suggests that cold matter intercepts a smaller part of the hard continuum in the fainter state of the source. On the other hand, the smaller number of seed photons available for the hot plasma makes the Comptonization photon-starved, as expected from variations of the spectral index in the hard continuum. The same scaling applies to the correlation of the amount of reflection itself, which on the scale of the reprocessed flux gives no reflection when extrapolating F_{HC} to zero.

The maximum disc temperature in our fits is also correlated with the hard X-ray flux (Fig. 8b), consistent with earlier findings that the

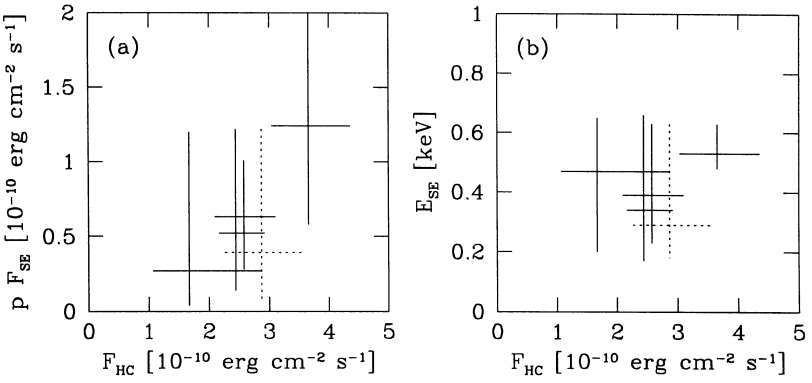

Figure 7. Correlation of (a) the total flux emitted in the soft excess, and (b) the cut-off energy of the soft excess component with the total flux emitted in the X/γ hard continuum. The plotted points come from the fits to the *Ginga* observations, which require the soft excess component at a confidence level greater than 0.95. The total flux emitted in the soft excess is positively correlated with that from the hard continuum (at a confidence level of 0.90), while the cut-off energy of the soft excess is consistent with being constant. The plotted pF_{SE} flux is the soft excess flux multiplied by a model-dependent factor, p, which cannot be determined from the available *Ginga* data (cf. Section 3.2 for discussion).

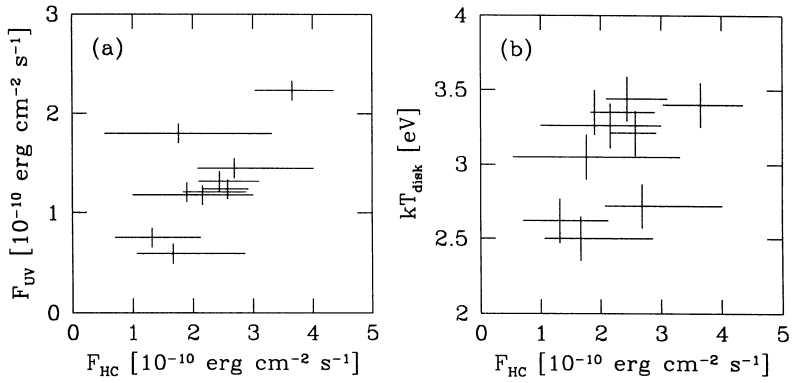

Figure 8. Correlation of (a) the total flux emitted in the disc component and (b) the maximum disc temperature with the total flux emitted in the X/γ hard continuum. The correlation is calculated under the assumption that the disc component constitutes all of the emission in the UV (cf. Fig. 5). A Spearman rank-order correlation test gives confidence levels of 0.96 and 0.89 for F_{HC} versus F_{UV} and F_{HC} versus kT_{disc}, respectively. F_{UV} does not contain the flux emitted in soft X-rays; thus, it underestimates the total flux emitted in the optical/UV/soft X-ray component, which in the average spectrum (cf. Fig. 5) is comparable to the total flux emitted in the hard X-ray continuum.

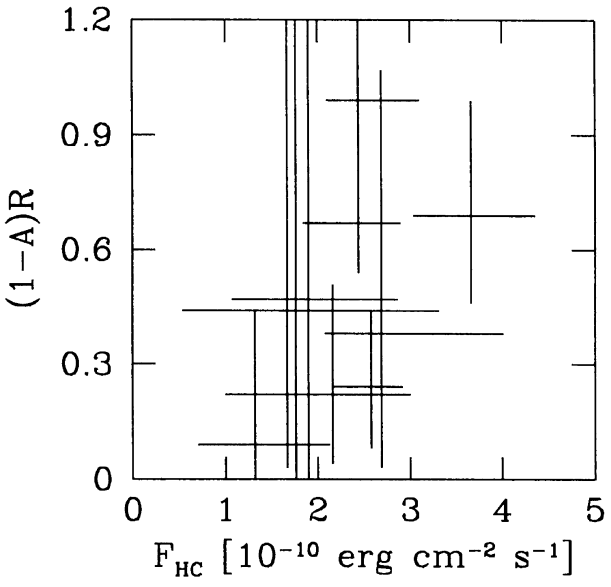

Figure 9. The fraction of the observed X/γ hard continuum $(1-A)R$ that is intercepted by the cold matter. The geometrical factor of the reprocessed flux has been neglected. The correlation is degraded compared with that expected from Fig. 6, because of the poor determination of the total flux emitted in the hard continuum.

UV spectrum becomes harder as the source brightens (e.g. Korista et al. 1995).

5 DISCUSSION AND CONCLUSIONS

To summarize, we have found that the overall optical/UV/ X/γ continuum can be deconvolved into three components: a cool multitemperature blackbody (presumably an accretion disc), a hard thermal Comptonized component from a hot plasma with modest optical depth (with reflection from the disc superposed), and an EUV/soft X-ray component which is well fitted by thermal Comptonization in a warm ($\sim$0.3 keV), optically thick medium. Parameters of the hot plasma inferred by the fit ($\tau \sim 2$, $kT_{HC} \sim 50$ keV) are consistent with those obtained from broad-band fits to NGC 4151 data (Zdziarski et al. 1996), and with those suggested from the average spectra of Seyferts (Zdziarski et al. 1997). The fluxes in all three components are positively correlated. In addition, as the source gets brighter, the optical/UV spectrum hardens while the hard continuum softens. Both the soft excess and hard continuum cut-off energies are consistent with being constant. Finally, the amount of reflection increases as the source brightens, requiring that the disc intercepts a greater fraction of the hard continuum.

The last correlation is perhaps the most interesting, because it suggests that variability in this source is connected to variability in the geometry of the continuum emission regions. One can easily rationalize some of the trends using this fact. Suppose for example that some process redistributes matter in the disc so that it intercepts (and reflects) more of the hard continuum. This would imply greater X-ray heating of the disc material, producing a brighter, harder optical/UV continuum. The increased number of seed photons would then increase the cooling of the X/γ corona, producing a larger hard continuum flux. Provided the heating of the hot Comptonizing plasma does not rise quickly, the hard X-ray continuum would then soften. Enhanced Compton cooling has also been proposed to explain unusually steep hard X-ray spectra in other Seyfert galaxies (e.g. Pounds, Done & Osborne 1995). In addition (or alternatively), the softer hard continuum may be caused by a drop in the scattering depth of the hot medium. Thus, in the bright state the optical/UV and X/γ continua are radiatively coupled. On the other hand, in the faint state the two components asymptotically decouple because of the small solid angle of the cold matter seen by the X/γ source (Fig. 9). In this state, most of the optical/UV emission might come from viscous heating in the disc, although our data do not allow for a proper deconvolution of the energetics.

One possibility for variations in the source geometry which would be consistent with the observations is a change of the inner edge of the disc connected to thermal/viscous instabilities near the innermost stable orbit or to instabilities in a transition region to a central hot disc (cf. Magdziarz & Blaes 1998). Such a central disc could be related to an advection-dominated accretion flow and might itself contain UV-emitting cloudlets (cf. Haardt 1997, and references therein). A decrease of the inner edge radius would of course produce an increase in the observed maximum disc temperature and optical/UV flux, and would also cause intercepting and reflecting more of the X/γ continuum. However, an excess in the amount of reflection suggested from the fits requires some

deviations from the plane parallel geometry of cold matter. Otherwise, the hot plasma, which has optical depth ~ 2, would Comptonize away most of the reflected photons, thereby erasing the reflection component. Recently, Abramowicz, Igumenshchev & Lasota (1998) have shown that the transition region between the cold disc (Shakura & Sunyaev 1973) and the hot advection-dominated disc (Ichimaru 1977) should indeed have complex dynamical structure. Their two-dimensional hydrodynamical simulations show vortices and circulations of matter related to convective instability of viscous flow in the disc transition region.

The conical wind model (Walter & Courvoisier 1990) has problems explaining the observed variability of the solid angle of the cold matter seen from the hot source (Fig. 6b), unless we assume a high propagation velocity of the active region (e.g. $\sim 0.1c$) in the cone and an extremely small diameter ($\sim 10R_{\rm g}$) of the accretion disc. Such relativistic propagation is consistent with non-thermal emission models (e.g. Ghisellini et al. 1991; Turner et al. 1993). However, such models seem to be rejected by the (apparently) thermal cut-off observed by OSSE in NGC 5548 and in other Seyfert galaxies generally, together with the strong limits on the presence of annihilation lines (Zdziarski et al. 1997). On the other hand, the annihilation line may be strongly suppressed by reacceleration of non-thermal particles in the hot source, leading to models basically consistent with observations (Henri & Petrucci 1997; Petrucci & Henri 1997; Petrucci et al. 1997).

Real progress in understanding the variability can only be made after understanding the true nature of the energetically important soft excess. If the soft excess is actually related to optically thick Comptonization, the entire big blue bump and the soft excess may be dominated by the same component (Fig. 5b). This would explain both the tight *IUE–EUVE* correlation (Marshall et al. 1997), and the absence of a Lyman edge in the UV spectrum (Kriss et al. 1997). It is noteworthy that thermal Comptonization also provides a good fit to the EUV/soft X-ray component of quasars (Zheng et al. 1997; Laor et al. 1997). Such a spectral continuum shape is incompatible with models invoking reprocessing by X-ray-illuminated or photo-ionized cold matter (e.g. Ross & Fabian 1993), unless substantial smearing of atomic features appearing in the EUV/soft X-ray range is assumed. Such smearing may come both from a complex emitting medium, with some stratification of physical parameters, and from relativistic transfer effects. However, a contribution from a distant reprocessor seems to be unlikely, since it cannot be substantially smeared and cannot produce the apparent positive correlation between the hard X-ray continuum and the Compton reflection component. The fact that thermal Comptonization fits to the soft excess require high optical depths also suggests that the Comptonization occurs within the inner regions of the disc itself (e.g. Maraschi & Molendi 1990). It is interesting that Kaastra & Barr (1989) also suggested that the observed variability in the *EXOSAT* data is consistent with the soft X-rays being produced in an inner, hot part of the disc. How to reconcile this with the changes in source geometry inferred from the variable reflection component is an unsolved problem which we leave to a future paper.

We believe that our spectral decomposition is the best that can be done with the available data, and further improvements can only be made after the acquisition of simultaneous spectral data which fully cover all three continuum components of NGC 5548.

ACKNOWLEDGMENTS

We are grateful to Chris Done, the referee of this paper, for supplying us with *ROSAT* data and for helpful comments. We are also grateful to Robert Antonucci, Todd Hurt and Greg Madejski for useful discussions. This work was supported in part by the Polish KBN grants 2P03D00514, 2P03D00614, 2P03C00511p01 and 2P03C00511p04, NSF grant AST 95-29230, and by NASA grants and contracts. This research has made use of data obtained through the High Energy Astrophysics Science Archive research Center Online Service, provided by the NASA/Goddard Space Flight Center, the ESA Villafranca Satellite Tracking Station, and the Leicester Database and Archive Service at the Department of Physics and Astronomy, Leicester University, UK.

REFERENCES

Abramowicz M. A., Igumenshchev I. V., Lasota J.-P., 1998, MNRAS, 293, 443
Agol E., Hubeny I., Blaes O., 1998, in Holt S. S., Kallman T., eds, Accretion Processes in Astrophysical Systems: Some Like It Hot. AIP, p. 175
Anders E., Ebihara M., 1982, Geochim. Cosmochim. Acta, 46, 2363
Antonucci R., 1993, ARA&A, 31, 473
Arnaud K. A., 1996, in Jacoby G., Barnes J., eds, ASP Conf. Ser. Vol. 101, Astronomical Data Analysis Software and Systems V. Astron. Soc. Pac., San Francisco, p. 17
Barvainis R., 1993, ApJ, 412, 513
Blaes O. M., 1998, in Holt S. S., Kallman T. R., eds, Accretion Processes in Astrophysical Systems: Some Like It Hot. AIP, p. 161
Branduardi-Raymont G., 1986, in Mason K. O., Watson M. G., White N. E., eds, The Physics of Accretion onto Compact Objects. Springer, Berlin, p. 407
Branduardi-Raymont G., 1989, in Osterbrock D. E., Miller J. S., eds, IAU Symp. 134, Active Galactic Nuclei. Kluwer, Dordrecht, p. 177
Cardelli J. A., Clayton G. C., Mathis J. S., 1989, ApJ, 345, 245
Clavel J. et al., 1991, ApJ, 366, 64
Clavel J. et al., 1992, ApJ, 393, 113
Coleman G. D., Wu C.-C., Weedman D. W., 1980, ApJS, 43, 393
Czerny B., Elvis M., 1987, ApJ, 321, 305
Czerny B., Życki P., 1994, ApJ, 431, L5
Done C., Mulchaey J. S., Mushotzky R. F., Arnaud K. A., 1992, ApJ, 395, 275
Done C., Pounds K. A., Nandra K., Fabian A. C., 1995, MNRAS, 275, 417
Edelson R. A. et al., 1996, ApJ, 470, 364
Fiore F., Elvis M., McDowell J. C., Siemiginowska A., Wilkes B., 1994, ApJ, 431, 515
Fiore F., Matt G., Nicastro F., 1997, MNRAS, 284, 731
George I. M., Turner T. J., Netzer H., Nandra K., Mushotzky R. F., Yaqoob T., 1998, ApJS, 114, 73
Ghisellini G., George I. M., Fabian A. C., Done C., 1991, MNRAS, 248, 14
Gondek D., Zdziarski A. A., Johnson W. N., Georgee I. M., McNaron-Brown K., Magdziarz P., Smith D., Gruber D. E., 1996, MNRAS, 282, 646
Górecki A., Wilczewski W., 1984, Acta Astron., 34, 141
Haardt F., 1997, in Comastri A., Venturi T., Bellazzini M., eds, From Micro to Mega Parsec. Mem. Soc. Astron. It., 68, 73
Haardt F., Maraschi L., 1991, ApJ, 380, L51
Haardt F., Maraschi L., Ghisellini G., 1994, ApJ, 432, L95
Haardt F., Maraschi L., Ghisellini G., 1997, ApJ, 476, 620
Henri G., Petrucci P. O., 1997, A&A, 326, 87
Ichimaru S., 1977, ApJ, 214, 840
Johnson W. N., Zdziarski A. A., Madejski G. M., Paciesas W. S., Steinle H., Lin Y.-C., 1997a, in Dermer Ch. D., Strickman M. S., Kurfess J. D., eds, AIP Conf. Proc. 410, Proceedings of the Fourth Compton Symposium. AIP, Woodbury NY, p. 283
Johnson W. N., McNaron-Brown K., Kurfess J. D., Zdziarski A. A., Magdziarz P., Gehrels N., 1997b, ApJ, 482, 173
Kaastra J. S., Barr P., 1989, A&A, 226, 59
Kallman T. R., 1998, in Proc. 2nd Oak Ridge Conference on Astrophysics. APS, in press
Kendall M. G., Stuart A., 1976, The Advanced Theory of Statistics, Vol. 3. Griffin & Co, London

Korista K. T. et al., 1995, ApJS, 97, 285
Kriss G., Krolik J., Grimes J., Tsvetanov Z., Espey B., Zheng W., Davidsen A., 1997, in Peterson B. M., Cheng F.-Z., Wilson A. S., eds, ASP Conf. Ser. Vol. 113, Emission Lines in Active Galaxies: New Methods and Techniques. Astron. Soc. Pac., San Francisco, p. 453
Krolik J. H., 1998, in Abramowicz M. A., Björnsson G., Pringle J. E., eds, Theory of Black Hole Accretion Discs, Cambridge Univ. Press, Cambridge, in press
Krolik J. H., Kallman T. R., 1984, ApJ, 286, 366
Krolik J. H., Horne K., Kallman T. R., Malkan M. A., Edelson R. A., Kriss G. A., 1991, ApJ, 371, 541
Kuraszkiewicz J., Loska Z., Czerny B., 1997, Acta Astron., 47, 263
Laor A., Fiore F., Elvis M., Wilkes B. J., McDowell J. C., 1997, ApJ, 477, 93
Lightman A. P., White T. R., 1988, ApJ, 335, 57
Lightman A. P., Zdziarski A. A., 1987, ApJ, 319, 643
Loska Z., Czerny B., 1997, MNRAS, 284, 946
Maciołek-Niedźwiecki A., Magdziarz P., 1998, in Chakrabarti S. K., ed, Observational Evidence for Black Holes in the Universe. Kluwer, Dordrecht, p. 231
Magdziarz P., Blaes O., 1998, in IAU Symp. 188, The Hot Universe. Kluwer, Dordrecht, in press
Magdziarz P., Zdziarski A. A., 1995, MNRAS, 273, 837
Maraschi L., Molendi S., 1990, ApJ, 353, 452
Marshall H. L. et al., 1997, ApJ, 479, 222
Mathur S., Elvis M., Wilkes B., 1995, ApJ, 452, 230
Matt G., Fabian A. C., Ross R. R., 1993, MNRAS, 264, 839
Matt G., Perola G. C., Piro L., 1991, A&A, 247, 25
Molendi S., Maraschi L., Stella L., 1992, MNRAS, 255, 27
Mushotzky R. F., Fabian A. C., Iwasawa K., Kunieda H., Matsuoka M., Nandra K., Tanaka Y., 1995, MNRAS, 272, L9
Nandra K., Pounds K. A., 1994, MNRAS, 268, 405
Nandra K., Pounds K. A., Stewart G. C., George I. M., Hayashida K., Makino F., Ohashi T., 1991, MNRAS, 248, 760
Nandra K. et al., 1993, MNRAS, 260, 504
Nandra K., Turner T. J., George I. M., Fabian A. C., Shrader C., Sun W.-H., 1995, MNRAS, 273, 85
Nandra K., George I. M., Mushotzky R. F., Turner T. J., Yaqoob T., 1997, ApJ, 477, 602
Osborne J., 1993, *ROSAT* UK Newsletter, 6, 7
Paltani S., Walter R., 1996, A&A, 312, 55
Papadakis I. E., Lawrence A., 1993, Nat, 361, 233
Peterson B. M. et al., 1992, ApJ, 392, 470
Petrucci P. O., Henri G., 1997, A&A, 326, 99
Petrucci P. O., Henri G., Malzac J., Jourdain E., 1997, in Dermer Ch. D., Strickman M. S., Kurfess J. D., eds, AIP Conf. Proc. 410, Proceedings of the Fourth Compton Symposium. AIP, Woodbury NY, p. 1303
Pounds K. A., Done C., Osborne J. P., 1995, MNRAS, 277, L5
Pozdnyakov L. A., Sobol' I. M., Sunyaev R. A., 1983, Astrophys. Space Phys. Rev., 2, 189
Reynolds C. S., Begelman M. C., 1997, ApJ, 488, 109
Romanishin W. et al., 1995, ApJ, 455, 516
Ross R. R., Fabian A. C., 1993, MNRAS, 261, 74
Ross R. R., Fabian A. C., Mineshige S., 1992, MNRAS, 258, 189
Shakura N. I., Sunyaev R. A., 1973, A&A, 24, 337
Sincell M. W., Krolik J. H., 1997, ApJ, 476, 605
Smith D. A., Done C., 1996, MNRAS, 280, 355
Tagliaferri G., Bao G., Israel G. L., Stella L., Treves A., 1996, ApJ, 465, 181
Turner T. J., Pounds K. A., 1989, MNRAS, 240, 833
Turner T. J. et al., 1993, ApJ, 407, 556
Walter R., Courvoisier T. J.-L., 1990, A&A, 233, 40
Walter R., Fink H. H., 1993, A&A, 274, 105
Walter R., Orr A., Courvoisier T. J.-L., Fink H. H., Makino F., Otani C., Wamsteker W., 1994, A&A, 285, 119
Warwick R. S. et al., 1996, ApJ, 470, 349
Witt H. J., Czerny B., Życki P. T., 1997, MNRAS, 288, 848
Yaqoob T., Warwick R. S., Makino F., Otani C., Sokolski J. L., Bond I. A., Yamauchi M., 1993, MNRAS, 262, 435
Zdziarski A. A., Magdziarz P., 1996, MNRAS, 279, L21
Zdziarski A. A., Johnson W. N., Done C., Smith D., McNaron-Brown K., 1995, ApJ, 438, L63
Zdziarski A. A., Johnson W. N., Magdziarz P., 1996, MNRAS, 283, 193
Zdziarski A. A., Johnson W. N., Poutanen J., Magdziarz P., Gierliński M., 1997, in Winkler Ch., Courvoisier T. J.-L., Durouchoux Ph., eds, The Transparent Universe, ESA SP-382. ESA, Noordwijk, p. 373
Zheng W., Kriss G. A., Telfer R. C., Grimes J. P., Davidsen A. F., 1997, ApJ, 475, 469
Życki P. T., Krolik J. H., Zdziarski A. A., Kallman T. R., 1994, ApJ, 437, 597

This paper has been typeset from a $\TeX$/$\LaTeX$ file prepared by the author.